HHS Public Access

Author manuscript

Tomography. Author manuscript; available in PMC 2016 May 23.

Published in final edited form as:

Tomography. 2016 March ; 2(1): 3–16. doi:10.18383/j.tom.2016.00121.

Radioactive Nanomaterials for Multimodality Imaging

Daiqin Chen[1,2], **Casey A. Dougherty**[1,2], **Dongzhi Yang**[1,2], **Hongwei Wu**[1,2], and **Hao Hong**[1,2,3,*]

[1]Department of Radiology, University of Michigan-Ann Arbor, Michigan 48109-2200, United States

[2]Center for Molecular Imaging, University of Michigan-Ann Arbor, Michigan 48109-2200, United States

[3]Comprehensive Cancer Center, University of Michigan-Ann Arbor, Michigan 48109-2200, United States

Abstract

Nuclear imaging techniques, including primarily positron emission tomography (PET) and single-photon emission computed tomography (SPECT), can provide quantitative information for a biological event in vivo with ultra-high sensitivity, however, the comparatively low spatial resolution is their major limitation in clinical application. By convergence of nuclear imaging with other imaging modalities like computed tomography (CT), magnetic resonance imaging (MRI) and optical imaging, the hybrid imaging platforms can overcome the limitations from each individual imaging technique. Possessing versatile chemical linking ability and good cargo-loading capacity, radioactive nanomaterials can serve as ideal imaging contrast agents. In this review, we provide a brief overview about current state-of-the-art applications of radioactive nanomaterials in the circumstances of multimodality imaging. We present strategies for incorporation of radioisotope(s) into nanomaterials along with applications of radioactive nanomaterials in multimodal imaging. Advantages and limitations of radioactive nanomaterials for multimodal imaging applications are discussed. Finally, a future perspective of possible radioactive nanomaterial utilization is presented for improving diagnosis and patient management in a variety of diseases.

Keywords

radioactive nanomaterials; multimodality imaging; PET; SPECT; MRI; optical imaging; fluorescence; photoacoustic imaging; Raman imaging; review

[*]**Corresponding author:** Hao Hong, Department of Radiology, University of Michigan, 109 Zina Pitcher Place, A520 BSRB, Ann Arbor, MI 48109-2200, ; Email: hahong@med.umich.edu

CONFLICT OF INTEREST

The authors declare no conflicts of interest for this article content.

1. INTRODUCTION

Molecular imaging has become a powerful tool for diagnosis and staging of multiple diseases and longitudinal treatment response monitoring (1-3). Imaging techniques, such as magnetic resonance imaging (MRI), computed tomography (CT), ultrasound (US), optical imaging, and nuclear imaging, are widely used in different clinical scenarios (4). However, each individual imaging modality has inherent drawbacks (5, 6) thus obtaining precise diagnostic information could be hampered by the use of a single imaging modality (7). Combining the merits of multiple imaging methods can provide for improved functional/anatomical information to be obtained thus researchers are more often utilizing multimodality imaging platforms for their synergistic readouts (8, 9).

Integration of nuclear imaging approaches with other imaging modalities (10, 11) is rapidly advancing as nuclear imaging (e.g. positron emission tomography [PET] and single-photon emission computed tomography [SPECT]) provide whole-body detection with unparalleled sensitivity, good tissue penetration, and quantitative capacity (12, 13), with extremely high clinical value (13, 14). However, PET and SPECT imaging suffer from poorer spatial resolution thus, the integration of PET or SPECT with other imaging methods with high spatial resolution, such as CT (15-18), and more recently MRI (19), provides synergistic opportunities for improved clinical diagnosis and overall patient care (11, 20). An interesting fact is that there has not been many standalone PET scanners sold in the marketplace since the introduction of PET/CT in 2001 (8), therefore the combination of PET and CT has become the “gold standard” for oncological imaging. With better soft tissue contrast and lower radiation dose than CT, MRI becomes a new attractive choice to integrate with PET (21), and this integration can help to compensate for the low molecular sensitivity/specificity of MRI (22, 23). Optical imaging (e.g. fluorescence), on the other hand, is less costly and provides real-time intraoperative guidance after the disease location is pinpointed by PET (or SPECT) (24).

Contrast agents, which can enhance image conspicuity for lesion detection, are desirable for improving molecular imaging sensitivity and specificity. For example, gadolinium compounds (typically T_1-weighted) and iron oxide materials (typically T_2-weighted) are commonly utilized MRI contrast agents (25, 26). Since PET and SPECT imaging rely on the detection of γ-photons (511 keV pair or spontaneous) emitted from radioactive isotopes (e.g. ^{18}F [$t_{1/2}$ = 110 min], ^{64}Cu [$t_{1/2}$ = 12.7 h], ^{89}Zr [$t_{1/2}$ = 78.4 h], and ^{99m}Tc [$t_{1/2}$ = 6 h] etc.) (12-14), the administration of contrast agents is indispensable. For successful multimodal imaging, a contrast agent with reliable performance and detectability by each imaging modality would be preferred. To achieve this goal, nanomaterials are very promising contrast agent candidates (27-29). The main advantages of nanomaterials include the following facts: 1) Some nanomaterials are inherent contrast agents as for example, iron oxide nanoparticles (IONPs) which have received approval by US food and drug administration (FDA) as MRI contrast agents (30, 31). 2) Most nanomaterials possess large surface areas, so they can accommodate numerous contrast agent molecules thereby increasing local concentration and detection sensitivity (32). 3) Different functional groups or active sites on nanomaterials enable them to be chemically linked to contrast agents or disease-targeting ligands (33). 4) Some nanomaterials can respond to specific stimuli (e.g.

heat, light, or pH fluctuation etc.) for on-demand release of payloads, which may improve the contrast in a given region of interest where the stimuli exist (34). 5) Nanomaterials can show selective accumulation in some disease sites. The well-known example is that nanomaterials with suitable size and morphology can distribute preferably at the tumor site through an enhanced permeation and retention (EPR) effect (27). Hence, multimodality imaging agents based on nanomaterials have undergone continuous improvements by research investigators (29).

An overview of the current state-of-the-art applications for radioactive nanomaterials as multimodality imaging contrast agents is provided by **Table 1**. As the availability of PET scanners has become wider in clinics and the sensitivity of PET is higher than SPECT, we will focus more on the radioactive nanomaterials applicable for PET-multimodality imaging while also providing a brief summary on nanomaterials useful for SPECT. With the rapid development of each imaging technique and nanotechnology, we foresee that radioactive nanomaterials will eventually be adopted as irreplaceable clinical tools in near future.

2. RADIOACTIVE NANOMATERIAL PRODUCTION

According to the chemical compositions, nanomaterials are classified into organic and inorganic nanomaterials. Common examples of organic nanomaterials include liposomes, polymers and dendrimers (35), and chemical compositions from inorganic nanoparticle families include silica, iron oxide, gold, and carbon-based nanomaterials (30, 36-38). Nanomaterials from both categories are useful tools for PET or SPECT fused multimodal imaging. To produce radioactive nanomaterials for imaging applications, four approaches have been undertaken to incorporate radioisotopes. 1) An exogenous coordination compound (named a “chelator”) is added onto the nanomaterial to bind radioactive metal ions (39). 2) Proton or neutron beams are used to bombard given atoms inside the nanomaterials to create post-synthesis radiolabels (40). 3) Radioactive precursors (or pre-radiolabeled building blocks) are employed to from radioactive nanomaterials (41, 42). 4) Isotope absorption or exchange is used for post-synthesis radiolabeling (43, 44).

Each isotope incorporation approach has its own advantages and limitations. The attachment of the radioactive metal ions via exogenous chelators is simple, efficient, and can be achieved at relatively low cost. However, the stability of resulting radiolabels has been a significant concern for this method, as radio-metals can potentially be released from the chelator by isotope trans-chelation, and chelators themselves can be dissociated from the nanomaterial via enzymatic interactions *in vivo*. Chemical instability can compromise accurate evaluation of the pharmacokinetic behavior of radioactive nanomaterials *in vivo*. Direct radiolabeling methods by proton/neutron bombardment can largely avoid above concerns, but the high cost and complicated instrumentation hinders practical use (40). While the radioactive precursor method can form highly stable radioactive nanomaterials for imaging applications, unfortunately the high radiation exposure during the production procedures is a significant working hazard (45). The chelator-free post-synthetic radiolabeling approach is a recently emerging method with low production cost and simplicity, although the stability and production yield of the resulting radioactive nanomaterials requires further improvement, and its application is currently limited to only a

few nanomaterials. For future development, an optimal production method for radioactive nanomaterials should have high yields, stable products, short reaction time, low radiation exposure, and be easily adaptable to most nanomaterials (45). Development of new production methods and improvements of current strategies will promote new applications of radioactive nanomaterials. The current review presents an overview of nanomaterials used in the context of their applicable imaging modality as shown in **Scheme 1**.

3. MULTIMODALITY IMAGING WITH RADIOACTIVE NANOMATERIALS

3.1 PET/MRI

The first instrument to combine PET and MRI together was developed in 2008 (19). Currently, both functional and anatomical data can be collected simultaneously by a modern PET/MRI scanner (46). Integration of PET and MRI endows the system with both high resolution and high sensitivity thus precise localization of the radioactive signals can be visualized within the context of anatomical features. Although a significant technical challenge, MRI can now provide attenuation correction for PET with clinically acceptable accuracy compared with CT-based attenuation correction (47-49). Due to the sensitivity differences between the two imaging modalities, dual modality contrast agents must take into account the need to maintain a relatively low concentration of PET contrast (usually within nanomolar range) along with a relatively high concentration of MRI contrast agent needed for sufficient MRI detection. Therefore, radioactive nanomaterials used in PET/MRI applications should ideally contain a sufficiently high MRI contrast ability along with a sufficient dose of radioactivity for PET detection. As a standout example, IONPs coupled with different isotopes served as the core of many PET/MRI imaging nanoplatforms (30).

3.1.1 IONPs—Since IONPs have been approved by the FDA as clinically usable contrast agents for MRI (commercial name ferumoxytol), radioactive IONPs serve as the most popular PET/MRI agents (50). Given the fact that benefits and limitations of radiolabeled IONPs as dual-modality SPECT/MRI and PET/MRI imaging probes have already been summarized elsewhere (51), here we will briefly provide recent examples of IONP applications. Zirconium-89 (^{89}Zr), a PET isotope with a decay half-life (78.4 h) is well matched to the circulation half-lives of antibodies or nanomaterials, as such, it is considered clinically relevant and has been reported in significant research activities over the last decade (52). ^{89}Zr-labeled ferumoxytol was used recently for PET/MRI mapping of tumor-drained lymph nodes (LN) in mice since LN invasion is both critical for cancer staging and important for treatment planning (53). ^{89}Zr was attached to ferumoxytol via ultra-stable coordination with desferrioxamine (DFO) (**Figure 1A**), and the modification of ferumoxytol core with ^{89}Zr-DFO did not alter its physicochemical properties such as size, charge and magnetic properties. ^{89}Zr-DFO-ferumoxytol provided sensitive tomographic detection of the tumor-drained axillary LN in prostate tumor-bearing mice with high resolution (**Figure 1A**). Compared with the commonly used agent (^{99m}Tc-radiocolloid) for LN mapping, ^{89}Zr-DFO-ferumoxytol shortened diagnosis time and decreased radiation dose to the test subjects. IONP-based platform has significant translational potential to improve preoperative planning for nodal resection and tumor staging. By coupling with different PET isotopes

(e.g. ^{64}Cu, ^{124}I, ^{72}As and ^{69}Ge), successful LN mapping was also achieved with these radioactive IONPs (54-57).

Aside from LN mapping, radioactive IONPs can also be used for *in vivo* cancer targeting. For example, arginine-glycine-aspartic (RGD, a potent ligand for integrin $\alpha_v\beta_3$) peptide-conjugated, ^{64}Cu-labeled IONPs could efficiently accumulate inside different types of tumor and give clear tumor delineation in both PET and MRI (58-60). More recently, hybrid nanostructures of IONPs (e.g. with aluminum hydroxide [labeled with ^{18}F] (61) or MoS_2 nanosheets [labeled with ^{64}Cu, **Figure 1B**] (62)) were also prepared for cancer imaging and subsequent image-guided cancer therapies. IONPs based PET/MRI agents still possess certain drawbacks. Since IONPs are mostly employed as T_2-weighted contrast agents (negative contrast), image interpretation can be relatively difficult. Another concern is the aggregation of IONPs in vivo, which can alter the local signal intensity from MRI. A recent study demonstrated that aggregated IONPs instead of IONPs alone, could produce significant artifacts in MR-derived attenuation correction maps from PET/MRI (63). To overcome these limitations, T_1-weighted contrast agents, e.g. gadolinium (Gd) and manganese (Mn) complexes, may be more preferred.

3.1.2 Gadolinium-containing nanomaterials—Gadolinium-containing nanomaterials are attractive MRI probes, as long as proper functionalization has been carried out to maintain material integrity and prevent leakage of Gd ions. As an image contrast platform, the applicability of gadolinium oxide nanoparticles in PET/MRI and therapeutic delivery has been reviewed recently (64).

Fullerene is also a well-known delivery vector of Gd (38). A PET/MRI probe based on ^{124}I labeled $Gd_3N@C_{80}$ fullerene derivate was developed and avoided potential cytotoxicity from Gd leakage by caging the gadolinium ions inside the fullerene structure (25). Not only can this biocompatible $Gd_3N@C_{80}$ be used as a T_1-weighted MRI agent and PET probe, it can also serve as a “radical sponge” to ameliorate inflammatory responses. Hydroxyl and carboxylic groups on the surface of $Gd_3N@C_{80}$ are also useful as they allow the capability of additional functionalization. Tumors inside glioblastoma-bearing rats could be distinctly visualized by ^{124}I-labeled $Gd_3N@C_{80}$ from both PET and MRI. Rare-earth nanomaterials are another category of suitable nanoplatform for PET/MRI applications (65). Among them, Eu^{3+}-doped gadolinium vanadate ($GdVO_4$:Eu) nanosheets which have been synthesized by a solvothermal reaction in one study and further modified by 1,4,7,10-tetraazacyclododecane-1,4,7,10-tetraacetic acid (DOTA) for ^{64}Cu labeling and Asp-Gly-Glu-Ala (DGEA) peptide for integrin $\alpha_2\beta_1$ cellular targeting (66). Prominent accumulation of ^{64}Cu-DOTA-$GdVO_4$:Eu-DGEA in PC-3 tumors (integrin $\alpha_2\beta_1^+$) was confirmed by both PET and MRI (**Figure 2A**) and tumor uptake was primarily mediated by integrin $\alpha_2\beta_1$ targeting. In an interesting study, a ^{64}Cu-labeled hybrid nanomaterial based on gold, Gd, and IONP was employed for dual T_1- and T_2-weighted MRI and PET to delineate tumors (67). The resultant hybrid heterotrimers showed high physiological stability and could induce simultaneous positive and negative contrast enhancements in MR images. PET imaging studies revealed that the hybrid heterostructures displayed favorable tumor delineation in mice, consistent with MRI findings.

There are rather limited reports available on Gd-containing organic nanomaterials as PET/MRI agents. One such example is Gd-containing liposome (68). In this study, Gd was introduced via diethylenetriaminepentaacetic acid (DTPA) coordination and ^{89}Zr was incorporated by adsorption on lipid membranes. Octreotide, a peptide targeting human somatostatin receptor subtype 2 (SSTR2), was also linked to the liposome complex. Clearly higher accumulation and retention in SSTR2^{+} tumors (acquired from PET/MRI), when compared with SSTR2^{-} tumors in the same animal, were strong evidence that these ^{89}Zr/Gd-containing liposomes demonstrated excellent tumor targeting ability *in vivo*. More recently, a glucose-based polymeric dextran nanomaterial (named "nanobeacon" by the authors) were also developed to retain ^{89}Zr and gadolinium in a chelator-free manner (69). These ^{89}Zr-nanobeacons could detect sentinel lymph nodes and allow the surveillance of drug release from nanobeacons via MRI, since MR signal from gadolinium could be quenched by the loaded drug on the nanobeacons.

3.1.3 Manganese-containing nanomaterials—The T_1-shortening properties qualify manganese as an MRI contrast agent (70). However, its biological toxicity hampered the development of otherwise useful applications such as cancer imaging, cell tracking, and brain imaging (71). Unlike gadolinium, an effective chelating agent with satisfactory binding stability for manganese has unfortunately not yet been identified for *in vivo* applications. Manganese-containing nanomaterials with sufficient *in vivo* stability may grant new biomedical applications to manganese. Surprisingly, using manganese-containing nanomaterials for PET/MRI is a current underexplored niche in contrast agent imaging research.

To the best of our knowledge, only one existing report has used ^{64}Cu-labeled, human serum albumin (HSA) coated MnO nanoparticles for PET/MRI imaging of glioblastoma (72). The coating of HSA can increase the solubility of MnO nanoparticles and their longitudinal r_1 relaxivity. These ^{64}Cu-labeled MnO@HSA nanoparticles demonstrated good physiological properties and stability along with superior T_1 contrast. Tumor accumulation from ^{64}Cu-labeled MnO@HSA was confirmed by both PET and MRI (**Figure 2B**). There are plenty of opportunities ahead for manganese-containing nanomaterials to be used in PET/MRI studies, since the production of ^{52}Mn ($t_{1/2}$ = 5.6 d) has been optimized for PET applications (73). For future development, radiolabeled hollow MnO nanoparticles (with better water accessibility) and stimulus-responsive manganese-containing nanomaterials are anticipated to both be useful for improving contrast agent sensitivity and specificity for detection of specific stimuli (74).

3.2 PET/optical

3.2.1 PET/fluorescence (luminescence)—The combination of PET and fluorescence/luminescence provides opportunities for radioactive nanomaterials to be used for fluorescence/luminescence-guided surgery post initial detection of the disease site(s) via PET. There are three categories of radioactive nanomaterials useful for PET/fluorescence. In the first category, the nanomaterial has intrinsic fluorescence (e.g. quantum dots (QD), gold nanomaterials, up-conversion nanoparticles [UCNP] etc.), which can be used for PET/fluorescence post direct radiolabeling. The second category involves nanomaterials labeled

with both a radioisotope and a fluorophore. Sometimes the loaded drugs (e.g. doxorubicin) on the nanomaterial can also serve as a fluorophore for imaging purposes (75-77). A third category involves radioactive nanomaterials that can be detected by both PET and Cerenkov luminescence imaging (CLI) from the same radiolabel. CLI is an emerging optical imaging modality based on the detection of Cerenkov radiation induced by particles emitted by a radioisotope as they travel through biological samples with a velocity faster than the speed of light (78). The progress in these three categories will be the focus of this section.

Radiolabeled QDs are the most prevalent nanomaterials for PET/fluorescence. QDs with different radiolabels (e.g. ^{64}Cu (79, 80) or ^{18}F (81)) have been used for PET/fluorescence imaging of tumor vasculature with consistent readouts from both PET and fluorescence imaging modalities. Rare-earth UCNP is another type of nanomaterial with unique intrinsic fluorescence. It can absorb low-energy photons and emit high energy photons (upconversion luminescence (UCL)), which results in a very optimal signal-to-background ratio for imaging (82). UCNPs are ideal building blocks for multimodal imaging probes. For example, ^{18}F-labeled, cyclodextrin-coated UCNPs were used for cell labeling and *in vivo* LN imaging via UCL/PET (83). The good biocompatibility from UCNPs encourages them to be used as multimodal imaging probes, although more reliable instrumentation will likely be needed for applications in UCL imaging. Other candidates such as red fluorescence emitting zinc oxide nanoparticles (84) can also be useful for PET/fluorescence.

Post-synthesis incorporation of both fluorophore and radioisotopes are most frequently adopted techniques to produce PET/fluorescence suited nanomaterials. For example, fluorescence-mediated tomography (FMT) and PET were used to measure protease activity, macrophage content and integrin expression simultaneously in tumor by using a biocompatible IONP with ^{18}F and a near-infrared (NIR) fluorophore attachment (85). Good correlations were shown between FMT and PET in probe concentration and spatial distribution of signals.

Silica-based nanomaterials are important for PET/fluorescence imaging, where a lot of attention has been devoted on mesoporous silica nanoparticles (MSNs) and ultra-small silica-based Cornell dots (C-dots). MSNs conjugated with ^{64}Cu, 800CW (a NIRF dye), and a monoclonal antibody, were adopted for PET/NIRF imaging of the tumor vasculature in one study (86). Good tumor targeting efficacy and specificity in breast tumor-bearing mice was achieved for this ^{64}Cu-labeled MSN, validated by PET and fluorescence. C-dots are the first PET/fluorescence nanoprobe that entered clinical stage testing. After conjugation with ^{124}I, an NIRF fluorophore (Cy5), and RGD peptide, C-dots were used as an integrin-targeting platform for imaging of melanoma metastasis with improved SLN localization and retention (**Figure 3A**), target-to-background ratios, and fast clearance from the site of injection and the body (87). The specificity of this C-Dots platform, when compared with ^{18}F-FDG, for metastasis/inflammation discrimination, was also satisfactory in the setting of surgery and therapeutic intervention. Furthermore, these radiolabeled C-dots were also used in a first-in-human clinical trial for lesion detection, cancer staging, and treatment management of patients with metastatic melanoma (88). ^{124}I-RGD-C-dots(Cy5) exhibited superior *in vivo* stability, reproducible pharmacokinetic signatures (renal excretion), good tolerance in patients, and sensitive detection of small metastatic lesions (**Figure 3A**).

As stated previously, CLI enables the use of widespread luminescence rodent imaging equipment (e.g. IVIS Spectrum) to visualize many commonly used medical isotopes (78), including clinical diagnostic (e.g. PET) and therapeutic radionuclides. Compared to conventional optical imaging agents, CLI enables the use of approved radiotracers and does not require an external light excitation source, which would result in its rapid translation to clinical applications combining PET imaging and CLI-guided surgery with PET tracers. An emerging concept is to produce self-illuminating imaging agents (Cerenkov luminescence from isotopes served as the excitation source – named Cerenkov resonance energy transfer (CRET)) without autofluorescence background interference. Currently, only a few self-illuminating probes were developed, based mainly on quantum dots (89, 90), and $^{64}CuCl_2$ was used as a synthesis precursor. These ^{64}Cu-doped QDs demonstrated excellent radiochemical stability and potent tumor uptake (**Figure 3B**), and were successfully applied as efficient imaging agents for PET/self-illuminating luminescence *in vivo*. Radioactive gold nanocluster (^{64}Cu-doped AuNCs) was another strong competitor for CRET-based PET/NIRF imaging (44), in which AuNCs acted as the energy acceptor for NIR fluorescence. ^{64}Cu-doped AuNCs exhibited efficient CRET-NIR and PET signals, better passive targeting to tumors, and lower toxicity than QD conjugates. Although these studies were conducted in a preclinical setting (mostly mouse studies), the successful clinical translation of CLI-nanomaterials can be expected in the future which will catapult radioactive nanomaterials towards increasingly versatile applications (91).

3.2.2 Other PET/optical imaging—Compared with fluorescence imaging, other optical imaging techniques, such as Raman imaging or photoacoustic imaging, can also provide opportunities for integration as hybrid imaging applications with PET. Since its discovery, Raman spectroscopy, based on the inelastic scattering of a photon, has proven to be a powerful analytical tool offering many advantages including excellent sensitivity to small structural and chemical changes, its ability to multiplex, and its resistance to both autofluorescence and photobleaching (92). Although radiolabeled noble metal nanomaterials and carbon nanomaterials can both be used for PET/Raman imaging, most of the time Raman imaging is only a safeguard to ensure that material distribution information collected from PET is accurate. For example, the organ distribution of ^{64}Cu-labeled gold nanoparticles was evaluated in mice by PET, and validated by *ex vivo* Raman imaging via surface-enhanced Raman scattering (SERS) (93). Raman imaging of excised tissues correlated well with distribution data from PET in this study (**Figure 4A**). The benefit of fusing Raman images onto PET images is that this combination can provide simultaneous surveillance of different materials/substances (with distinct Raman emissions) with excellent sensitivity (PET and Raman).

Photoacoustic imaging (PAI), based on the photoacoustic effect, is another attractive optical imaging technique with nonionizing electromagnetic waves, good resolution and contrast, portable instrumentation, and the ability to partially quantify the signal. PAI has been applied to the imaging of cancer, neurological disorders, vasculature function, and gene expression, among others (94). An anisotropic branched gold nanomaterial (Au-tripods) with superior optical properties was developed for PET/PAI (95). Linear correlation between PAI signals and Au-tripods concentration was confirmed *in vivo*. Intravenous administration

of ^{64}Cu-labeled, RGD peptide conjugated Au-tripods (RGD-Au-tripods) to U87MG tumor-bearing mice showed PAI contrast in tumors almost 3-fold higher than for the blocking group, and PAI results correlated well with corresponding PET images. Au-tripods demonstrated adequate selectivity and sensitivity for tumor in PET/PAI. In another study, the intrinsic PA signals and strong chelating properties (e.g. for ^{64}Cu) of melanin nanoparticle (MNP) were exploited to construct a PET/MRI/PAI agent (96). With apoferritin conjugation for transferrin receptor 1 (TfR1) targeting, this MNP showed excellent stability and presented good tumor uptake and high tumor contrast in HT29 tumor (TfR1^{+}) with significantly lower accumulation in HepG2 (TfR1^{-}, **Figure 4B**).

3.3 Multimodality imaging

Multimodality imaging platforms that combine more than two different imaging modalities have come into research focus (97, 98). To achieve this, nanomaterials used are usually in a hybrid structure or a core/shell architecture to embrace more contrast capacity from different components (99-101).

Cui and colleagues proposed two core-shell nanomaterials for trimodal (MRI, PET/SPECT and optical) imaging based on the integration of IONP and UCNP (102). The nanoparticles are composed of a core/shell Fe_3O_4@$NaYF_4$ nanoparticles with different metal ions doped (Yb, Er, Tm etc.). With the stabilization from polyethylene glycol, the obtained nanoparticles showed high transverse relaxivity (r_2) (326 $mM^{-1}s^{-1}$ at magnetic field of 3T), good radiolabel stability, and strong upconversion luminescence. LNs in live mice could be clearly visualized by using ^{18}F labeled Fe_3O_4@$NaYF_4$ (Yb, Tm) nanoparticles in PET, MRI, and UCL. With a similar design, hybrid gold-IONP nanoparticles were made, in which IONPs worked as a T_2 MRI contrast agent, and the gold component acted as a strong fluorescence emitter and functionalization site (modified with 1,4,7-triazacyclononane-1,4,7-trisacetic acid [NOTA] for ^{64}Cu labeling) (99). Anti-EGFR affibody was also included to provide tumor targeting capabilities. As expected, the gold-IONP platform gave very sharp tumor contrast in PET, MRI, and fluorescence imaging. More recently, another more dramatic example is the hexamodal imaging by porphyrin-phospholipids coated UCNP (PoP-UCNP) (103). To more fully utilize the imaging capacity of this nanomaterial, the authors characterized it both *in vitro* and *in vivo* for imaging via fluorescence, upconversion, PET, CT, CLI, and PAI (**Figure 5**).

3.4 SPECT-related multimodality imaging

For the last few decades, SPECT is the leading nuclear imaging technique due to the extensive use of ^{99m}Tc ($t_{½}$ = 6 h), which can be conveniently obtained from ^{99}Mo/^{99m}Tc generators (104). It is more established, less expensive, and more widely available than PET. One of the major advantages of SPECT imaging is that it can be used for simultaneous imaging of different radionuclides via the energy identification of the gamma photons emitted (105), thereby enabling simultaneous visualization of parallel biological events, although such strategy is not frequently adopted. From a material point of view, the key difference between a PET applicable nanomaterial and a SPECT applicable nanomaterial are the specific radioisotopes used. Since PET possesses certain superiority (e.g. higher detection sensitivity, better spatial resolution, and better quantitative capacity etc.) and has

become increasingly popular in both preclinical and clinical settings, SPECT-applicable nanomaterials will not be discussed in detail in this article. Similar to PET isotope-included nanomaterials, radioactive nanomaterials can be used for SPECT/MRI, SPECT/optical, and additional combinations are possible (106-108).

SPECT/MRI can be extremely helpful to scrutinize the *in vivo* kinetics of radioactive nanomaterials (20, 106, 109, 110). For example, *in vivo* metabolism of PEG-modified ultra-small paramagnetic iron oxide nanoparticles (USPIO, one type of IONPs), after labeling by ^{99m}Tc, could be monitored by both SPECT and MRI (**Figure 6A**) (111). ^{99m}Tc-PEG-IONP possess a high r_1 relaxivity and a low r_2/r_1 to serve as an attractive T_1-weighted MRI contrast agent. IONP-combined multi-walled carbon nanotubes (MWCNTs) were also used for SPECT/MRI after further radiolabeled with ^{99m}Tc (112). Mouse imaging studies showed that the T_2 contrast ability of SPION-MWCNTs were comparable to that of the clinically approved MRI contrast agent, Endorem. Organ distribution of SPION-MWCNTs acquired from SPECT, along with *ex vivo* transmission electronic microscopy (TEM) and histological assessment, confirmed the integrity of SPION-MWCNTs in organs. Moreover, Gd-containing nanomaterials were also important participants for SPECT/MRI studies. For example, hybrid gadolinium oxide nanoparticles (obtained by encapsulating Gd_2O_3 cores within a polysiloxane shell), which carried fluorophore Cy5 and ^{111}In, were used in SPECT, fluorescence, and MRI to evaluate their metabolism (e.g. renal clearance) in rodents (113). A clear correlation was observed between modalities.

There are also plenty of radioactive nanomaterials useful for SPECT/fluorescence imaging or SPECT-involved multimodality imaging. Polymeric micelles conjugated with an EphB4 (a receptor tyrosine kinases overexpressed in many tumors)-binding peptide TNYL-RAW, a NIRF fluorophore Cy7, and ^{111}In, was used for tumor imaging via SPECT and NIRF (114). PC-3M tumors (EphB4$^+$) could be clearly visualized by both SPECT and NIRF tomography after intravenous administration of ^{111}In-labeled TNYL-RAW-micelles (**Figure 6B**). EphB4 specificity was confirmed from tumor uptake in A549 tumors (EphB4$^-$) and blocking experiments. Fluorescence signal from the nanoparticles correlated with their radioactivity count, and co-localized with the EphB4 expressing region from histology. Liposomes incorporated with fluorescence labels and Gd or ^{111}In, were investigated in optical, MRI and SPECT imaging for their cellular uptake and organ distribution (115). The ability to tune the imaging properties and distribution of these liposomes allows for the future development of a flexible tri-modal imaging agent. Other more recent progress includes optically tunable nanomaterials featuring a unique design where a single PEG polymer surrounds a fluorophore and radiometal bearing peptide (116). These nanomaterials could be applied for intraoperative angiography, measurements of capillary permeability, and tumor visualization by SPECT, for potential patient stratification.

4. SUMMARY AND FUTURE PERSPECTIVES

There are two critical composing elements for a radioactive nanomaterial, i.e. the radioisotope, and the nanomaterial. To make the radioactive nanomaterial readily applicable for multimodality imaging, the suitable selection of both components should be synergistic. On one hand, incorporation of radioisotope(s) bestows extra tracking/therapeutic ability to

the nanomaterial which cannot be acquired by loading of other cargos. On the other hand, the utilization of suitable nanomaterials may serve as an isotope carrier and enable some unconventional isotopes to be used in specific biomedical applications which might otherwise be very difficult to achieve, such as radioactive arsenic (e.g. ^{72}As) (57, 117), gemanium-69 (^{69}Ge) (56), or sodium-22 (^{22}Na) (118). Different imaging "labels" can be integrated into a single nanoplatform for combining the strengths of different imaging modalities, which can synergistically improve the overall value of imaging in the context of basic research or patient care. In addition, nanomaterials with appropriate functionalization can evade attack from the immune system and thus create prolonged imaging time (45). Moreover, since most nanomaterials have large surface areas which result in superior cargo accommodating capacity, they can help to increase local imaging contrast in selected areas. In addition, loading of imaging labels (isotopes/fluorophores etc.) in nanomaterials can cause alterations of the *in vivo* pharmacokinetics of the labels, which can be tunable for image optimization in most cases.

Each imaging modality has its own advantages and limits. For example, the high sensitivity and good quantitative capability provided by PET/SPECT accompanies their low spatial resolution (typical > 1 mm). The inherent low sensitivity of MRI and penetration limitations from optical imaging calls for combining the strengths of different imaging modalities to synergistically improve the information content that imaging can provide. When radioactive nanomaterials are used in multimodality imaging, their stability is one of the most crucial factors for detection reliability, accuracy and safety. The concept of "stability" here has dual meanings – radiochemical stability, and stability of the nanomaterial itself. To acquire reliable and comparable imaging results, all the cargo(s) (especially the radioisotopes) should stay adequately stable within the nanomaterial structure during the *in vivo* application, since PET or SPECT identifies the location of radionuclides rather than nanomaterials. Alternate functionalization/engineering strategies can be applied to not only optimize the stability of radioactive nanomaterials, but also to provide the possibility for conjugation of a diverse number of different biological and bioactive molecules including drugs, proteins, and targeting ligands (32).

Another major challenge for radioactive nanoparticles is in optimization of their effectiveness to target specific disease phenotypes (39). Significant reports on radioactive nanomaterials utilized passive targeting only based on the EPR effect, which is relying on the size, shape, surface charge, and circulation half-life of the nanoparticles. Although this can be therapeutically efficacious in some cases, this is by no means optimal for an imaging/diagnostic purpose. For example, the prolonged circulation half-life from a nanomaterial is a double-edged sword - although it can lead to higher level of passive targeting to the tumor, it also causes prolonged exposure of the normal organs to the drug/radioisotope which can give rise to undesired systemic toxicity. Active targeting is an approach that can enhance the preferential nanomaterial accumulation at disease site(s) via coupling with ligands that have selectivity and affinity toward diseased cells or tissues, or by a provided external stimulus (e.g. a magnetic field) on a target cell/tissue spatial location (119). We can expect significantly more research effort will be devoted to produce nanomaterials with active targeting capacity to improve multimodal image contrast. More specifically for oncological imaging, we believe that targeting of markers on tumor neovasculature will be more efficient

for radioactive nanomaterials since the size of many materials hinders their extravasation into the surrounding tumor parenchyma (120).

The majority of radioactive nanomaterials discussed in this article have a hydrodynamic size range of 10–200 nm, which can cause persistent accumulation in the mononuclear phagocyte system (MPS, e.g. liver and spleen). To ensure a long-term safety profile can be achieved, careful radiation dosimetry and toxicological evaluation for each radioactive nanomaterial should be accomplished (121). In the meantime, suitable biological properties should be engineered into the design of the nanomaterial (e.g. size/surface charge/degradability adjustment for fast renal clearance) in an effort to tune the *in vivo* distribution pattern to allow for injected contrast agents to be cleared within a reasonable period in order to meet subsequent FDA approval (122).

In summary, radioactive nanomaterials that can integrate multiple contrast agents into one single platform are important to realize real-time multimodality imaging. As multimodality imaging probes, radioactive nanomaterials should be able to provide for improved diagnostic accuracy. Continued research into the development of radioactive nanomaterials for imaging applications are anticipated to lead to for example, radiolabeled IONPs that will be useful in simultaneous PET/MRI for early cancer diagnosis and disease staging. There are numerous opportunities and underexplored areas in radioactive nanomaterial research (e.g. manganese nanomaterials), which we believe will serve as indispensable diagnostic and therapeutic tools in future medical applications. Overall, it is fully anticipated that continued advances in nanomaterials research will significantly improve clinical care and have a significant and positive impact on enhancing patient outcomes in the years ahead.

ACKNOWLEDGEMENT

This work is supported, in part, by the University of Michigan Department of Radiology, the Elsa U. Pardee Foundation, and the National Institutes of Health (NCI P01 CA085878).

Abbreviations

IONPs	iron oxide nanoparticles
DFO	desferrioxamine
UCL	upconversion luminescence
MWCNTs	multi-walled carbon nanotubes
PAI	photoacoustic imaging
CLI	Cerenkov luminescence imaging
QD	quantum dots
FMT	fluorescence-mediated tomography
MSNs	mesoporous silica nanoparticles
CRET	Cerenkov resonance energy transfer

REFERENCES

1. Weissleder R, Pittet MJ. Imaging in the era of molecular oncology. Nature. 2008; 452:580–589. [PubMed: 18385732]
2. Kurtz DM, Gambhir SS. Tracking cellular and immune therapies in cancer. Adv Cancer Res. 2014; 124:257–296. [PubMed: 25287692]
3. Pysz MA, Gambhir SS, Willmann JK. Molecular imaging: current status and emerging strategies. Clin Radiol. 2010; 65:500–516. [PubMed: 20541650]
4. James ML, Gambhir SS. A molecular imaging primer: modalities, imaging agents, and applications. Physiol Rev. 2012; 92:897–965. [PubMed: 22535898]
5. Lee D-E, Koo H, Sun I-C, Ryu JH, Kim K, Kwon IC. Multifunctional nanoparticles for multimodal imaging and theragnosis. Chem Soc Rev. 2012; 41:2656–2672. [PubMed: 22189429]
6. Huang Y, He S, Cao W, Cai K, Liang X-J. Biomedical nanomaterials for imaging-guided cancer therapy. Nanoscale. 2012; 4:6135–6149. [PubMed: 22929990]
7. Jennings LE, Long NJ. 'Two is better than one'—probes for dual-modality molecular imaging. Chem Commun. 2009:3511–3524.
8. Louie A. Multimodality imaging probes: design and challenges. Chem Rev. 2010; 110:3146–3195. [PubMed: 20225900]
9. Kim J, Piao Y, Hyeon T. Multifunctional nanostructured materials for multimodal imaging, and simultaneous imaging and therapy. Chem Soc Rev. 2009; 38:372–390. [PubMed: 19169455]
10. Culver J, Akers W, Achilefu S. Multimodality molecular imaging with combined optical and SPECT/PET modalities. J Nucl Med. 2008; 49:169–172. [PubMed: 18199608]
11. Rosales R. Potential clinical applications of bimodal PET MRI or SPECT MRI agents. J Label Compounds Radiopharm. 2014; 57:298–303.
12. Deri MA, Zeglis BM, Francesconi LC, Lewis JS. PET imaging with ^{89}Zr: from radiochemistry to the clinic. Nucl Med Biol. 2013; 40:3–14. [PubMed: 22998840]
13. Anderson CJ, Ferdani R. Copper-64 radiopharmaceuticals for PET imaging of cancer: advances in preclinical and clinical research. Cancer Biother Radiopharm. 2009; 24:379–393. [PubMed: 19694573]
14. Ametamey SM, Honer M, Schubiger PA. Molecular imaging with PET. Chem Rev. 2008; 108:1501–1516. [PubMed: 18426240]
15. Townsend DW, Carney JP, Yap JT, Hall NC. PET/CT today and tomorrow. J Nucl Med. 2004; 45:4S–14S. [PubMed: 14736831]
16. Townsend DW. A combined PET/CT scanner: the choices. J Nucl Med. 2001; 42:533–534. [PubMed: 11337536]
17. Nishioka T, Shiga T, Shirato H, Tsukamoto E, Tsuchiya K, Kato T, Ohmori K, Yamazaki A, Aoyama H, Hashimoto S. Image fusion between ^{18}FDG-PET and MRI/CT for radiotherapy planning of oropharyngeal and nasopharyngeal carcinomas. Int J Rad Oncol Biol Phys. 2002; 53:1051–1057.
18. Bar-Shalom R, Yefremov N, Guralnik L, Gaitini D, Frenkel A, Kuten A, Altman H, Keidar Z, Israel O. Clinical performance of PET/CT in evaluation of cancer: additional value for diagnostic imaging and patient management. J Nucl Med. 2003; 44:1200–1209. [PubMed: 12902408]
19. Pichler BJ, Judenhofer MS, Catana C, Walton JH, Kneilling M, Nutt RE, Siegel SB, Claussen CD, Cherry SR. Performance test of an LSO-APD detector in a 7-T MRI scanner for simultaneous PET/MRI. J Nucl Med. 2006; 47:639–647. [PubMed: 16595498]
20. Bouziotis P, Psimadas D, Tsotakos T, Stamopoulos D, Tsoukalas C. Radiolabeled iron oxide nanoparticles as dual-modality SPECT/MRI and PET/MRI agents. Curr Topics Med Chem. 2012; 12:2694–2702.
21. Judenhofer MS, Wehrl HF, Newport DF, Catana C, Siegel SB, Becker M, Thielscher A, Kneilling M, Lichy MP, Eichner M. Simultaneous PET-MRI: a new approach for functional and morphological imaging. Nature Med. 2008; 14:459–465. [PubMed: 18376410]
22. Hofmann M, Pichler B, Schölkopf B, Beyer T. Towards quantitative PET/MRI: a review of MR-based attenuation correction techniques. Eur J Nucl Med Mol imaging. 2009; 36:93–104.

23. Antoch G, Bockisch A. Combined PET/MRI: a new dimension in whole-body oncology imaging? Eur J Nucl Med Mol imaging. 2009; 36:113–120.
24. Hussain T, Nguyen QT. Molecular imaging for cancer diagnosis and surgery. Adv Drug Deliv Rev. 2014; 66:90–100. [PubMed: 24064465]
25. Luo J, Wilson JD, Zhang J, Hirsch JI, Dorn HC, Fatouros PP, Shultz MD. A dual PET/MR imaging nanoprobe: 124I labeled $Gd_3N@C_{80}$. Appl Sci. 2012; 2:465–478.
26. Cowger, T.; Xie, J. Nanomaterial Interfaces in Biology. Springer; 2013. Polyaspartic acid coated iron oxide nanoprobes for PET/MRI imaging; p. 225-235.
27. Hahn MA, Singh AK, Sharma P, Brown SC, Moudgil BM. Nanoparticles as contrast agents for in-vivo bioimaging: current status and future perspectives. Anal Bioanal Chem. 2011; 399:3–27. [PubMed: 20924568]
28. Liang R, Wei M, Evans DG, Duan X. Inorganic nanomaterials for bioimaging, targeted drug delivery and therapeutics. Chem Commun. 2014; 50:14071–14081.
29. Barreto JA, O'Malley W, Kubeil M, Graham B, Stephan H, Spiccia L. Nanomaterials: applications in cancer imaging and therapy. Adv Mater. 2011; 23:H18–H40. [PubMed: 21433100]
30. Ai F, Ferreira CA, Chen F, Cai W. Engineering of radiolabeled iron oxide nanoparticles for dual modality imaging. Wiley Interdisciplinary Rev Nanomed Nanobiotechnol. 2015 Epub.
31. Lee J-H, Kim J.-w. Cheon J. Magnetic nanoparticles for multi-imaging and drug delivery. Mol Cell. 2013; 35:274–284.
32. Liu Z, Kiessling F, Gätjens J. Advanced nanomaterials in multimodal imaging: design, functionalization, and biomedical applications. J Nanomater. 2010; 2010:51.
33. Biju V. Chemical modifications and bioconjugate reactions of nanomaterials for sensing, imaging, drug delivery and therapy. Chem Soc Rev. 2014; 43:744–764. [PubMed: 24220322]
34. Portney NG, Ozkan M. Nano-oncology: drug delivery, imaging, and sensing. Anal Bioanal Chem. 2006; 384:620–630. [PubMed: 16440195]
35. Ahmed N, Fessi H, Elaissari A. Theranostic applications of nanoparticles in cancer. Drug Discovery Today. 2012; 17:928–934. [PubMed: 22484464]
36. Chen Y, Chen H, Shi J. In vivo bio-safety evaluations and diagnostic/therapeutic applications of chemically designed mesoporous silica nanoparticles. Adv Mater. 2013; 25:3144–3176. [PubMed: 23681931]
37. Alex S, Tiwari A. Functionalized Gold Nanoparticles: Synthesis, Properties and Applications--A Review. J Nanosci Nanotechnol. 2015; 15:1869–1894. [PubMed: 26413604]
38. Chen D, Dougherty CA, Zhu K, Hong H. Theranostic applications of carbon nanomaterials in cancer: Focus on imaging and cargo delivery. J Control Release. 2015; 210:230–245. [PubMed: 25910580]
39. Hong H, Zhang Y, Sun J, Cai W. Molecular imaging and therapy of cancer with radiolabeled nanoparticles. Nano Today. 2009; 4:399–413. [PubMed: 20161038]
40. Gibson N, Holzwarth U, Abbas K, Simonelli F, Kozempel J, Cydzik I, Cotogno G, Bulgheroni A, Gilliland D, Ponti J. Radiolabelling of engineered nanoparticles for in vitro and in vivo tracing applications using cyclotron accelerators. Arch Toxicol. 2011; 85:751–773. [PubMed: 21479952]
41. Black KC, Wang Y, Luehmann HP, Cai X, Xing W, Pang B, Zhao Y, Cutler CS, Wang LV, Liu Y. Radioactive ^{198}Au-doped nanostructures with different shapes for in vivo analyses of their biodistribution, tumor uptake, and intratumoral distribution. ACS nano. 2014; 8:4385–4394. [PubMed: 24766522]
42. Wang Y, Liu Y, Luehmann H, Xia X, Wan D, Cutler C, Xia Y. Radioluminescent gold nanocages with controlled radioactivity for real-time in vivo imaging. Nano Lett. 2013; 13:581–585. [PubMed: 23360442]
43. Zhou M, Zhang R, Huang M, Lu W, Song S, Melancon MP, Tian M, Liang D, Li C. A chelator-free multifunctional [^{64}Cu] CuS nanoparticle platform for simultaneous micro-PET/CT imaging and photothermal ablation therapy. J Am Chem Soc. 2010; 132:15351–15358. [PubMed: 20942456]
44. Hu H, Huang P, Weiss OJ, Yan X, Yue X, Zhang MG, Tang Y, Nie L, Ma Y, Niu G. PET and NIR optical imaging using self-illuminating 64 Cu-doped chelator-free gold nanoclusters. Biomaterials. 2014; 35:9868–9876. [PubMed: 25224367]

45. Sun X, Cai W, Chen X. Positron Emission Tomography Imaging Using Radiolabeled Inorganic Nanomaterials. Acc Chem Res. 2015; 48:286–294. [PubMed: 25635467]
46. Pichler BJ, Kolb A, Nägele T, Schlemmer H-P. PET/MRI: paving the way for the next generation of clinical multimodality imaging applications. J Nucl Med. 2010; 51:333–336. [PubMed: 20150252]
47. Martinez-Möller A, Souvatzoglou M, Delso G, Bundschuh RA, Chefd'hotel C, Ziegler SI, Navab N, Schwaiger M, Nekolla SG. Tissue classification as a potential approach for attenuation correction in whole-body PET/MRI: evaluation with PET/CT data. J Nucl Med. 2009; 50:520–526. [PubMed: 19289430]
48. Keereman V, Fierens Y, Broux T, De Deene Y, Lonneux M, Vandenberghe S. MRI-based attenuation correction for PET/MRI using ultrashort echo time sequences. J Nucl Med. 2010; 51:812–818. [PubMed: 20439508]
49. Glaus C, Rossin R, Welch MJ, Bao G. In vivo evaluation of ^{64}Cu-labeled magnetic nanoparticles as a dual-modality PET/MR imaging agent. Bioconjug Chem. 2010; 21:715–722. [PubMed: 20353170]
50. Pablico-Lansigan MH, Situ SF, Samia AC. Magnetic particle imaging: advancements and perspectives for real-time in vivo monitoring and image-guided therapy. Nanoscale. 2013; 5:4040–4055. [PubMed: 23538400]
51. Bouziotis P, Psimadas D, Tsotakos T, Stamopoulos D, Tsoukalas C. Radiolabeled iron oxide nanoparticles as dual-modality SPECT/MRI and PET/MRI agents. Curr Top Med Chem. 2012; 12:2694–2702. [PubMed: 23339765]
52. Zhang Y, Hong H, Cai W. PET tracers based on Zirconium-89. Curr Radiopharm. 2011; 4:131–139. [PubMed: 22191652]
53. Thorek DL, Ulmert D, Diop N-FM, Lupu ME, Doran MG, Huang R, Abou DS, Larson SM, Grimm J. Non-invasive mapping of deep-tissue lymph nodes in live animals using a multimodal PET/MRI nanoparticle. Nature Commun. 2014:5.
54. Choi, J.s.; Park, JC.; Nah, H.; Woo, S.; Oh, J.; Kim, KM.; Cheon, GJ.; Chang, Y.; Yoo, J.; Cheon, J. A hybrid nanoparticle probe for dual modality positron emission tomography and magnetic resonance imaging. Angew Chem Int Ed. 2008; 47:6259–6262.
55. Torres Martin de Rosales R, Tavare R, Paul RL, Jauregui-Osoro M, Protti A, Glaria A, Varma G, Szanda I, Blower PJ. Synthesis of ^{64}Cu(II)-bis(dithiocarbamatebisphosphonate) and its conjugation with superparamagnetic iron oxide nanoparticles: in vivo evaluation as dual-modality PET-MRI agent. Angew Chem Int Ed Engl. 2011; 50:5509–5513. [PubMed: 21544908]
56. Chakravarty R, Valdovinos HF, Chen F, Lewis CM, Ellison PA, Luo H, Meyerand ME, Nickles RJ, Cai W. Intrinsically germanium-69-labeled iron oxide nanoparticles: synthesis and in-vivo dual-modality PET/MR imaging. Adv Mater. 2014; 26:5119–5123. [PubMed: 24944166]
57. Chen F, Ellison PA, Lewis CM, Hong H, Zhang Y, Shi S, Hernandez R, Meyerand ME, Barnhart TE, Cai W. Chelator-free synthesis of a dual-modality PET/MRI agent. Angew Chem Int Ed Engl. 2013; 52:13319–13323. [PubMed: 24166933]
58. Xie J, Chen K, Huang J, Lee S, Wang J, Gao J, Li X, Chen X. PET/NIRF/MRI triple functional iron oxide nanoparticles. Biomaterials. 2010; 31:3016–3022. [PubMed: 20092887]
59. Yang X, Hong H, Grailer JJ, Rowland IJ, Javadi A, Hurley SA, Xiao Y, Yang Y, Zhang Y, Nickles RJ, Cai W, Steeber DA, Gong S, cRGD-functionalized. DOX-conjugated, and ^{64}Cu-labeled superparamagnetic iron oxide nanoparticles for targeted anticancer drug delivery and PET/MR imaging. Biomaterials. 2011; 32:4151–4160. [PubMed: 21367450]
60. Lee HY, Li Z, Chen K, Hsu AR, Xu C, Xie J, Sun S, Chen X. PET/MRI dual-modality tumor imaging using arginine-glycine-aspartic (RGD)-conjugated radiolabeled iron oxide nanoparticles. J Nucl Med. 2008; 49:1371–1379. [PubMed: 18632815]
61. Cui X, Belo S, Kruger D, Yan Y, de Rosales RT, Jauregui-Osoro M, Ye H, Su S, Mathe D, Kovacs N, Horvath I, Semjeni M, Sunassee K, Szigeti K, Green MA, Blower PJ. Aluminium hydroxide stabilised $MnFe_2O_4$ and Fe_3O_4 nanoparticles as dual-modality contrasts agent for MRI and PET imaging. Biomaterials. 2014; 35:5840–5846. [PubMed: 24768194]
62. Liu T, Shi S, Liang C, Shen S, Cheng L, Wang C, Song X, Goel S, Barnhart TE, Cai W, Liu Z. Iron oxide decorated MoS_2 nanosheets with double PEGylation for chelator-free radiolabeling and

multimodal imaging guided photothermal therapy. ACS Nano. 2015; 9:950–960. [PubMed: 25562533]

63. Borra RJ, Cho HS, Bowen SL, Attenberger U, Arabasz G, Catana C, Josephson L, Rosen BR, Guimaraes AR, Hooker JM. Effects of ferumoxytol on quantitative PET measurements in simultaneous PET/MR whole-body imaging: a pilot study in a baboon model. EJNMMI Phys. 2015; 2:6. [PubMed: 26501808]
64. Kim TJ, Chae KS, Chang Y, Lee GH. Gadolinium oxide nanoparticles as potential multimodal imaging and therapeutic agents. Curr Top Med Chem. 2013; 13:422–433. [PubMed: 23432005]
65. Bouzigues C, Gacoin T, Alexandrou A. Biological applications of rare-earth based nanoparticles. ACS nano. 2011; 5:8488–8505. [PubMed: 21981700]
66. Hu H, Li D, Liu S, Wang M, Moats R, Conti PS, Li Z. Integrin alpha2beta1 targeted $GdVO_4$:Eu ultrathin nanosheet for multimodal PET/MR imaging. Biomaterials. 2014; 35:8649–8658. [PubMed: 25043573]
67. Cheng K, Yang M, Zhang R, Qin C, Su X, Cheng Z. Hybrid nanotrimers for dual T1 and T2-weighted magnetic resonance imaging. ACS Nano. 2014; 8:9884–9896. [PubMed: 25283972]
68. Abou DS, Thorek DL, Ramos NN, Pinkse MW, Wolterbeek HT, Carlin SD, Beattie BJ, Lewis JS. ^{89}Zr-labeled paramagnetic octreotide-liposomes for PET-MR imaging of cancer. Pharm Res. 2013; 30:878–888. [PubMed: 23224977]
69. Kaittanis C, Shaffer TM, Bolaender A, Appelbaum Z, Appelbaum J, Chiosis G, Grimm J. Multifunctional MRI/PET nanobeacons derived from the in situ self-assembly of translational polymers and clinical cargo through coalescent intermolecular forces. Nano Lett. 2015; 15:8032–8043. [PubMed: 26540670]
70. Jacobs KE, Behera D, Rosenberg J, Gold G, Moseley M, Yeomans D, Biswal S. Oral manganese as an MRI contrast agent for the detection of nociceptive activity. NMR Biomed. 2012; 25:563–569. [PubMed: 22447731]
71. Crossgrove J, Zheng W. Manganese toxicity upon overexposure. NMR Biomed. 2004; 17:544–553. [PubMed: 15617053]
72. Huang J, Xie J, Chen K, Bu L, Lee S, Cheng Z, Li X, Chen X. HSA coated MnO nanoparticles with prominent MRI contrast for tumor imaging. Chem Commun (Camb). 2010; 46:6684–6686. [PubMed: 20730157]
73. Graves SA, Hernandez R, Fonslet J, England CG, Valdovinos HF, Ellison PA, Barnhart TE, Elema DR, Theuer CP, Cai W, Nickles RJ, Severin GW. Novel preparation methods of ^{52}Mn for immunoPET imaging. Bioconjug Chem. 2015; 26:2118–2124. [PubMed: 26317429]
74. Hao Y, Wang L, Zhang B, Zhao H, Niu M, Hu Y, Zheng C, Zhang H, Chang J, Zhang Z, Zhang Y. Multifunctional nanosheets based on folic acid modified manganese oxide for tumor-targeting theranostic application. Nanotechnology. 2016; 27:025101. [PubMed: 26629735]
75. Chen F, Hong H, Shi S, Goel S, Valdovinos HF, Hernandez R, Theuer CP, Barnhart TE, Cai W. Engineering of hollow mesoporous silica nanoparticles for remarkably enhanced tumor active targeting efficacy. Sci Rep. 2014; 4:5080. [PubMed: 24875656]
76. Guo J, Hong H, Chen G, Shi S, Zheng Q, Zhang Y, Theuer CP, Barnhart TE, Cai W, Gong S. Image-guided and tumor-targeted drug delivery with radiolabeled unimolecular micelles. Biomaterials. 2013; 34:8323–8332. [PubMed: 23932288]
77. Xiao Y, Hong H, Javadi A, Engle JW, Xu W, Yang Y, Zhang Y, Barnhart TE, Cai W, Gong S. Multifunctional unimolecular micelles for cancer-targeted drug delivery and positron emission tomography imaging. Biomaterials. 2012; 33:3071–3082. [PubMed: 22281424]
78. Thorek D, Robertson R, Bacchus WA, Hahn J, Rothberg J, Beattie BJ, Grimm J. Cerenkov imaging - a new modality for molecular imaging. Am J Nucl Med Mol Imaging. 2012; 2:163–173. [PubMed: 23133811]
79. Chen K, Li Z-B, Wang H, Cai W, Chen X. Dual-modality optical and positron emission tomography imaging of vascular endothelial growth factor receptor on tumor vasculature using quantum dots. Eur J Nucl Med Mol imaging. 2008; 35:2235–2244. [PubMed: 18566815]
80. Cai W, Chen K, Li Z-B, Gambhir SS, Chen X. Dual-function probe for PET and near-infrared fluorescence imaging of tumor vasculature. J Nucl Med. 2007; 48:1862–1870. [PubMed: 17942800]

81. Ducongé F, Pons T, Pestourie C, Hérin L, Thézé B, Gombert K, Mahler B, Hinnen F, Kühnast B, Dollé F. Fluorine-18-labeled phospholipid quantum dot micelles for in vivo multimodal imaging from whole body to cellular scales. Bioconjugate Chem. 2008; 19:1921–1926.
82. Park YI, Lee KT, Suh YD, Hyeon T. Upconverting nanoparticles: a versatile platform for wide-field two-photon microscopy and multi-modal in vivo imaging. Chem Soc Rev. 2015; 44:1302–1317. [PubMed: 25042637]
83. Liu Q, Chen M, Sun Y, Chen G, Yang T, Gao Y, Zhang X, Li F. Multifunctional rare-earth self-assembled nanosystem for tri-modal upconversion luminescence/fluorescence/positron emission tomography imaging. Biomaterials. 2011; 32:8243–8253. [PubMed: 21820170]
84. Hong H, Wang F, Zhang Y, Graves SA, Eddine SB, Yang Y, Theuer CP, Nickles RJ, Wang X, Cai W. Red fluorescent zinc oxide nanoparticle: a novel platform for cancer targeting. ACS Appl Mater Interfaces. 2015; 7:3373–3381. [PubMed: 25607242]
85. Nahrendorf M, Keliher E, Marinelli B, Waterman P, Feruglio PF, Fexon L, Pivovarov M, Swirski FK, Pittet MJ, Vinegoni C. Hybrid PET-optical imaging using targeted probes. Proc Nat Acad Sci. 2010; 107:7910–7915. [PubMed: 20385821]
86. Chen F, Nayak TR, Goel S, Valdovinos HF, Hong H, Theuer CP, Barnhart TE, Cai W. In vivo tumor vasculature targeted PET/NIRF imaging with TRC105(Fab)-conjugated, dual-labeled mesoporous silica nanoparticles. Mol Pharm. 2014; 11:4007–4014. [PubMed: 24937108]
87. Bradbury MS, Phillips E, Montero PH, Cheal SM, Stambuk H, Durack JC, Sofocleous CT, Meester RJ, Wiesner U, Patel S. Clinically-translated silica nanoparticles as dual-modality cancer-targeted probes for image-guided surgery and interventions. Integr Biol. 2013; 5:74–86.
88. Phillips E, Penate-Medina O, Zanzonico PB, Carvajal RD, Mohan P, Ye Y, Humm J, Gonen M, Kalaigian H, Schoder H, Strauss HW, Larson SM, Wiesner U, Bradbury MS. Clinical translation of an ultrasmall inorganic optical-PET imaging nanoparticle probe. Sci Transl Med. 2014; 6:260ra149.
89. Sun X, Huang X, Guo J, Zhu W, Ding Y, Niu G, Wang A, Kiesewetter DO, Wang ZL, Sun S, Chen X. Self-illuminating ^{64}Cu-doped CdSe/ZnS nanocrystals for in vivo tumor imaging. J Am Chem Soc. 2014; 136:1706–1709. [PubMed: 24401138]
90. Guo W, Sun X, Jacobson O, Yan X, Min K, Srivatsan A, Niu G, Kiesewetter DO, Chang J, Chen X. Intrinsically radioactive [^{64}Cu]CuInS/ZnS quantum dots for PET and optical imaging: improved radiochemical stability and controllable Cerenkov luminescence. ACS Nano. 2015; 9:488–495. [PubMed: 25549258]
91. Thorek DL, Riedl CC, Grimm J. Clinical Cerenkov luminescence imaging of ^{18}F-FDG. J Nucl Med. 2014; 55:95–98. [PubMed: 24078721]
92. Zhang Y, Hong H, Cai W. Imaging with Raman spectroscopy. Curr Pharm Biotechnol. 2010; 11:654–661. [PubMed: 20497112]
93. Zavaleta CL, Hartman KB, Miao Z, James ML, Kempen P, Thakor AS, Nielsen CH, Sinclair R, Cheng Z, Gambhir SS. Preclinical evaluation of Raman nanoparticle biodistribution for their potential use in clinical endoscopy imaging. Small. 2011; 7:2232–2240. [PubMed: 21608124]
94. Zhang Y, Hong H, Cai W. Photoacoustic imaging. Cold Spring Harb Protoc. 2011:2011. [PubMed: 21363959]
95. Cheng K, Kothapalli SR, Liu H, Koh AL, Jokerst JV, Jiang H, Yang M, Li J, Levi J, Wu JC, Gambhir SS, Cheng Z. Construction and validation of nano gold tripods for molecular imaging of living subjects. J Am Chem Soc. 2014; 136:3560–3571. [PubMed: 24495038]
96. Yang M, Fan Q, Zhang R, Cheng K, Yan J, Pan D, Ma X, Lu A, Cheng Z. Dragon fruit-like biocage as an iron trapping nanoplatform for high efficiency targeted cancer multimodality imaging. Biomaterials. 2015; 69:30–37. [PubMed: 26275860]
97. Park JC, Yu MK, An GI, Park SI, Oh J, Kim HJ, Kim JH, Wang EK, Hong IH, Ha YS. Facile preparation of a hybrid nanoprobe for triple modality optical/PET/MR imaging. Small. 2010; 6:2863–2868. [PubMed: 21104828]
98. Kang KW. Preliminary pre-clinical results and overview on PET/MRI/fluorescent molecular imaging. Open Nucl Med J. 2010; 2:153–156.

99. Yang M, Cheng K, Qi S, Liu H, Jiang Y, Jiang H, Li J, Chen K, Zhang H, Cheng Z. Affibody modified and radiolabeled gold–iron oxide hetero-nanostructures for tumor PET, optical and MR imaging. Biomaterials. 2013; 34:2796–2806. [PubMed: 23343632]

100. Xie J, Chen K, Huang J, Lee S, Wang J, Gao J, Li X, Chen X. PET/NIRF/MRI triple functional iron oxide nanoparticles. Biomaterials. 2010; 31:3016–3022. [PubMed: 20092887]

101. Huang X, Zhang F, Lee S, Swierczewska M, Kiesewetter DO, Lang L, Zhang G, Zhu L, Gao H, Choi HS. Long-term multimodal imaging of tumor draining sentinel lymph nodes using mesoporous silica-based nanoprobes. Biomaterials. 2012; 33:4370–4378. [PubMed: 22425023]

102. Cui X, Mathe D, Kovács N, Horváth I, Jauregui-Osoro M, Torres Martin de Rosales R, Mullen GE, Wong W, Yan Y, Krüger D. Synthesis, Characterization, and Application of Core–Shell $Co_{0.16}Fe_{2.84}O_4$@ NaYF4 (Yb, Er) and Fe_3O_4@ $NaYF_4$ (Yb, Tm) Nanoparticle as Trimodal (MRI, PET/SPECT, and Optical) Imaging Agents. Bioconjug Chem. 2015 Epub.

103. Rieffel J, Chen F, Kim J, Chen G, Shao W, Shao S, Chitgupi U, Hernandez R, Graves SA, Nickles RJ, Prasad PN, Kim C, Cai W, Lovell JF. Hexamodal imaging with porphyrin-phospholipid-coated upconversion nanoparticles. Adv Mater. 2015; 27:1785–1790. [PubMed: 25640213]

104. Eckelman WC. Unparalleled contribution of technetium-99m to medicine over 5 decades. JACC Cardiovasc Imaging. 2009; 2:364–368. [PubMed: 19356582]

105. Berman DS, Kiat H, Van Train K, Friedman JD, Wang FP, Germano G. Dual-isotope myocardial perfusion SPECT with rest thallium-201 and stress Tc-99m sestamibi. Cardiol Clin. 1994; 12:261–270. [PubMed: 8033176]

106. Madru R, Kjellman P, Olsson F, Wingårdh K, Ingvar C, Ståhlberg F, Olsrud J, Lätt J, Fredriksson S, Knutsson L. ^{99m}Tc-labeled superparamagnetic iron oxide nanoparticles for multimodality SPECT/MRI of sentinel lymph nodes. J Nucl Med. 2012; 53:459–463. [PubMed: 22323777]

107. Lijowski M, Caruthers S, Hu G, Zhang H, Scott MJ, Williams T, Erpelding T, Schmieder AH, Kiefer G, Gulyas G. High-resolution SPECT-CT/MR molecular imaging of angiogenesis in the Vx2 model. Invest Radiol. 2009; 44:15. [PubMed: 18836386]

108. Zielhuis SW, Seppenwoolde J-H, Mateus VA, Bakker CJ, Krijger GC, Storm G, Zonnenberg BA, Schip A.D.v.h. Koning GA, Nijsen JF. Lanthanide-loaded liposomes for multimodality imaging and therapy. Cancer Biother Radiopharm. 2006; 21:520–527. [PubMed: 17105424]

109. Lee H-Y, Li Z, Chen K, Hsu AR, Xu C, Xie J, Sun S, Chen X. PET/MRI dual-modality tumor imaging using arginine-glycine-aspartic (RGD)–conjugated radiolabeled iron oxide nanoparticles. J Nucl Med. 2008; 49:1371–1379. [PubMed: 18632815]

110. Torres Martin de Rosales R, Tavaré R, Glaria A, Varma G, Protti A, Blower PJ. ^{99m}Tcbisphosphonate-iron oxide nanoparticle conjugates for dual-modality biomedical imaging. Bioconjugate Chem. 2011; 22:455–465.

111. Sandiford L, Phinikaridou A, Protti A, Meszaros LK, Cui X, Yan Y, Frodsham G, Williamson PA, Gaddum N, Botnar RM. Bisphosphonate-anchored PEGylation and radiolabeling of superparamagnetic iron oxide: long-circulating nanoparticles for in vivo multimodal (T_1 MRI-SPECT) imaging. ACS Nano. 2012; 7:500–512. [PubMed: 23194247]

112. Wang JTW, Cabana L, Bourgognon M, Kafa H, Protti A, Venner K, Shah AM, Sosabowski JK, Mather SJ, Roig A. Magnetically decorated multiwalled carbon nanotubes as dual MRI and SPECT contrast agents. Adv Funct Mater. 2014; 24:1880–1894. [PubMed: 26097444]

113. Kryza D, Taleb J, Janier M, Marmuse L, Miladi I, Bonazza P, Louis C, Perriat P, Roux S, Tillement O, Billotey C. Biodistribution study of nanometric hybrid gadolinium oxide particles as a multimodal SPECT/MR/optical imaging and theragnostic agent. Bioconjug Chem. 2011; 22:1145–1152. [PubMed: 21545181]

114. Zhang R, Xiong C, Huang M, Zhou M, Huang Q, Wen X, Liang D, Li C. Peptide-conjugated polymeric micellar nanoparticles for dual SPECT and optical imaging of EphB4 receptors in prostate cancer xenografts. Biomaterials. 2011; 32:5872–5879. [PubMed: 21612822]

115. Mitchell N, Kalber TL, Cooper MS, Sunassee K, Chalker SL, Shaw KP, Ordidge KL, Badar A, Janes SM, Blower PJ, Lythgoe MF, Hailes HC, Tabor AB. Incorporation of paramagnetic, fluorescent and PET/SPECT contrast agents into liposomes for multimodal imaging. Biomaterials. 2013; 34:1179–1192. [PubMed: 23131536]

116. Guo Y, Yuan H, Claudio NM, Kura S, Shakerdge N, Mempel TR, Bacskai BJ, Josephson L. PEG-like nanoprobes: multimodal, pharmacokinetically and optically tunable nanomaterials. Plos One. 2014; 9:e95406. [PubMed: 24781778]

117. Ellison PA, Barnhart TE, Chen F, Hong H, Zhang Y, Theuer CP, Cai W, Nickles RJ, DeJesus O. High yield production and radiochemical isolation of isotopically pure arsenic-72 and novel radioarsenic labeling strategies for the development of theranostic radiopharmaceuticals. Bioconjug Chem. 2015

118. Al Faraj A, Alotaibi B, Shaik AP, Shamma KZ, Al Jammaz I, Gerl J. Sodium-22-radiolabeled silica nanoparticles as new radiotracer for biomedical applications: in vivo positron emission tomography imaging, biodistribution, and biocompatibility. Int J Nanomedicine. 2015; 10:6293–6302. [PubMed: 26504381]

119. Yang Y, Yu C. Advances in silica based nanoparticles for targeted cancer therapy. Nanomedicine. 2015 Epub.

120. Hong H, Chen F, Zhang Y, Cai W. New radiotracers for imaging of vascular targets in angiogenesis-related diseases. Adv Drug Deliv Rev. 2014; 76:2–20. [PubMed: 25086372]

121. Khalili Fard J, Jafari S, Eghbal MA. A review of molecular mechanisms involved in toxicity of nanoparticles. Adv Pharm Bull. 2015; 5:447–454. [PubMed: 26819915]

122. Choi HS, Liu W, Liu F, Nasr K, Misra P, Bawendi MG, Frangioni JV. Design considerations for tumour-targeted nanoparticles. Nat Nanotechnol. 2010; 5:42–47. [PubMed: 19893516]

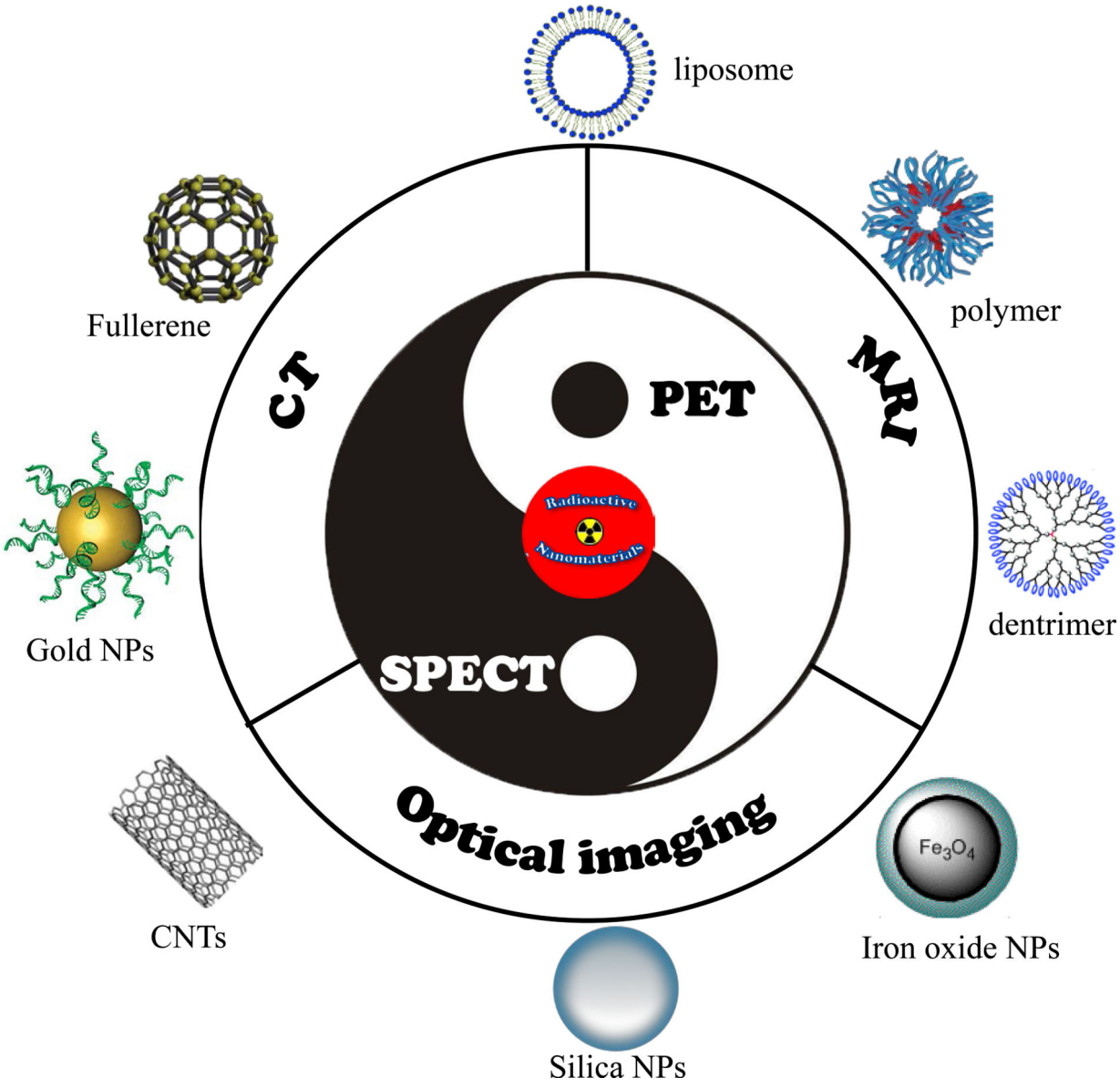

Scheme 1.
Schematic illustration of radioactive nanomaterials for multimodality imaging.

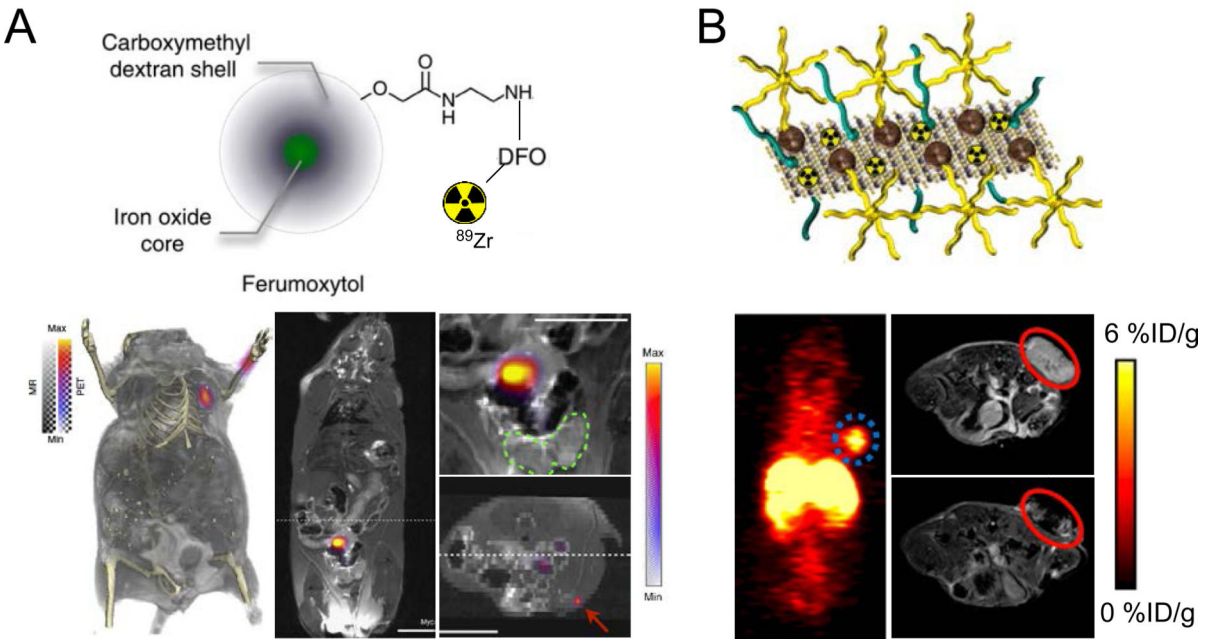

Figure 1.

(A) The application of ^{89}Zr-ferumoxytol for normal LNs and tumor-drained LNs. Top panel: the structure of ^{89}Zr-ferumoxytol. Lower left panel: detection of normal anxillary LNs by ^{89}Zr-ferumoxytol in PET/MRI. Lower middle panel: detection of tumor-drained LN in Hi-Myc mouse by ^{89}Zr-ferumoxytol in PET/MRI. Down right upper panel: PET/MRI of prostate region showing that the drained LN is outside of the prostate organ (green circle). Down right lower panel: distant drained inguinal node is identified by ^{89}Zr-ferumoxytol (red arrow). Adapted with permission (53). (B) The application of ^{64}Cu-labeled, MoS_2/IONP hybrid nanomaterial for PET and MRI based tumor detection. The structure of ^{64}Cu-labeled MoS_2/IONP is shown along with PET and MRI results at 24 h post-injection. Significant tumor uptake was confirmed in PET (circle indicates the tumor location) with “darkened” tumor area in MRI. Adapted with permission (62).

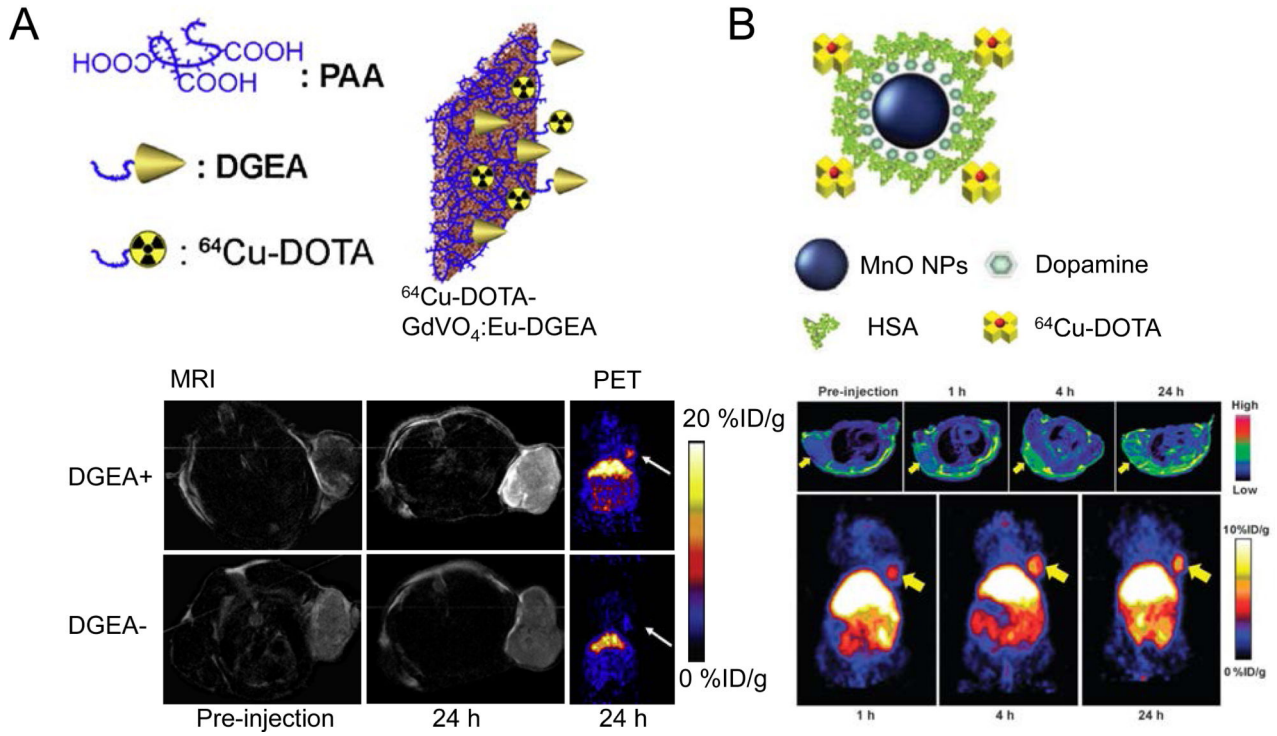

Figure 2.

(A) Application of ^{64}Cu-labeled $GdVO_4$:Eu nanosheets for targeted tumor imaging. The schematic structure of ^{64}Cu-DOTA-$GdVO_4$:Eu nanosheets is shown. PET and MRI images of PC-3 (EphB4$^+$) tumor-bearing mice at 24 h post-injection is shown for ^{64}Cu-DOTA-$GdVO_4$:Eu nanosheets with or without conjugation of DGEA peptide. Adapted with permission (66). (B) Application of ^{64}Cu-labeled MnO@HSA nanoparticles for MRI and PET imaging of tumors. Upper panel: MR images on U87MG xenografts acquired at 0, 1, 4 and 24 h after ^{64}Cu-labeled MnO@HSA injection. Lower panel: PET images taken at 1, 4 and 24 h after ^{64}Cu-labeled MnO@HSA injection. Adapted with permission (72).

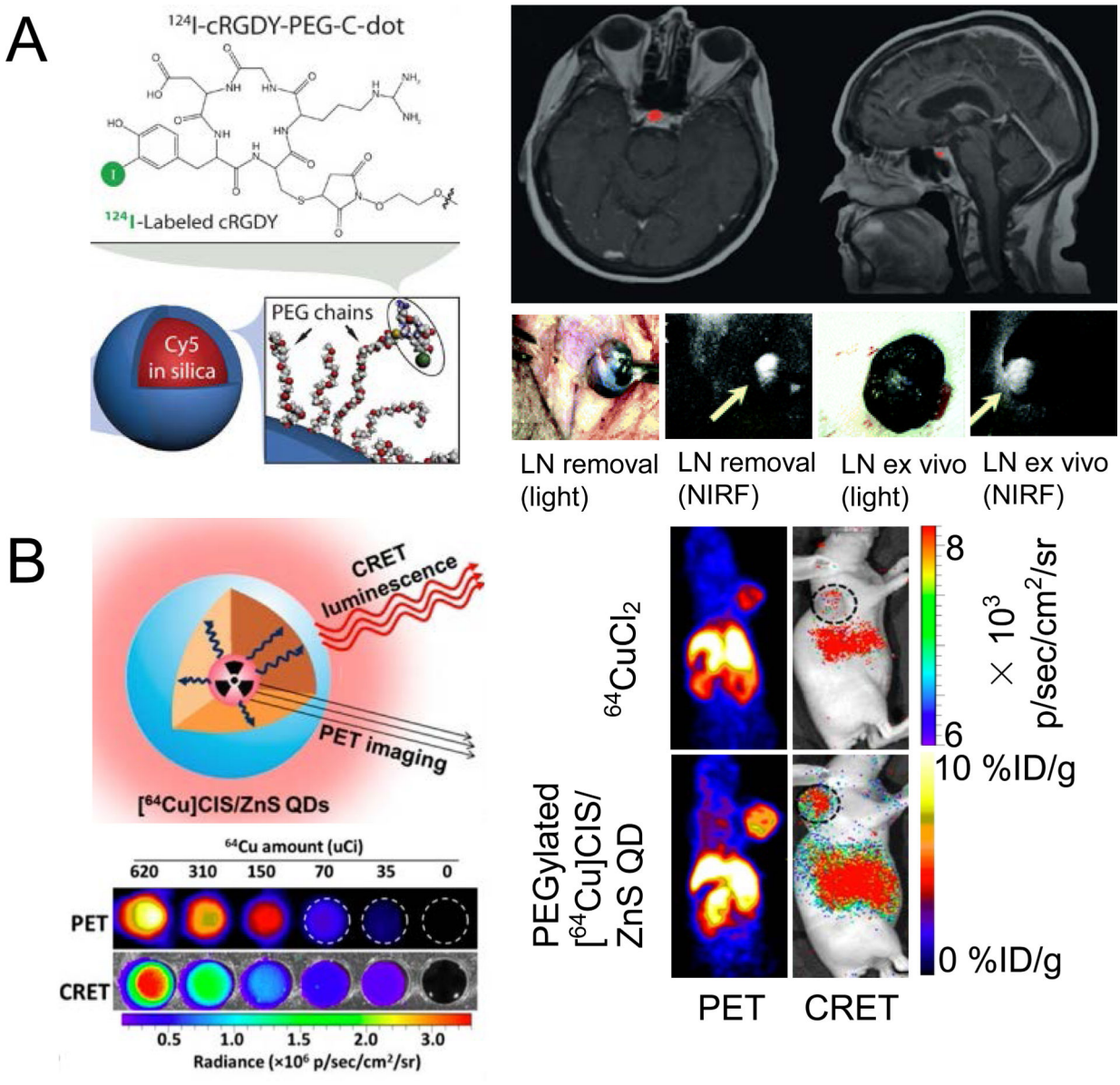

Figure 3.

(A) Application of ^{124}I-labeled, RGD-conjugated C-Dots for clinical cancer detection and NIRF-guided surgery. Biocompatible C-Dots could delineate small pituitary lesion in metastatic patient in PET/MRI. The same structured C-Dots were successfully used for NIRF-guided tumor-drained LN removal. Adapted with permission from references (87) and (88). (B) Structure and application of intrinsically radioactive ^{64}Cu-QDs for PET and CRET imaging. CRET luminescence photon flux was in a linear correlation with incorporated radioactivity. Consistent tumor uptake in U87MG tumors was revealed by PET and CRET. Adapted with permission (90).

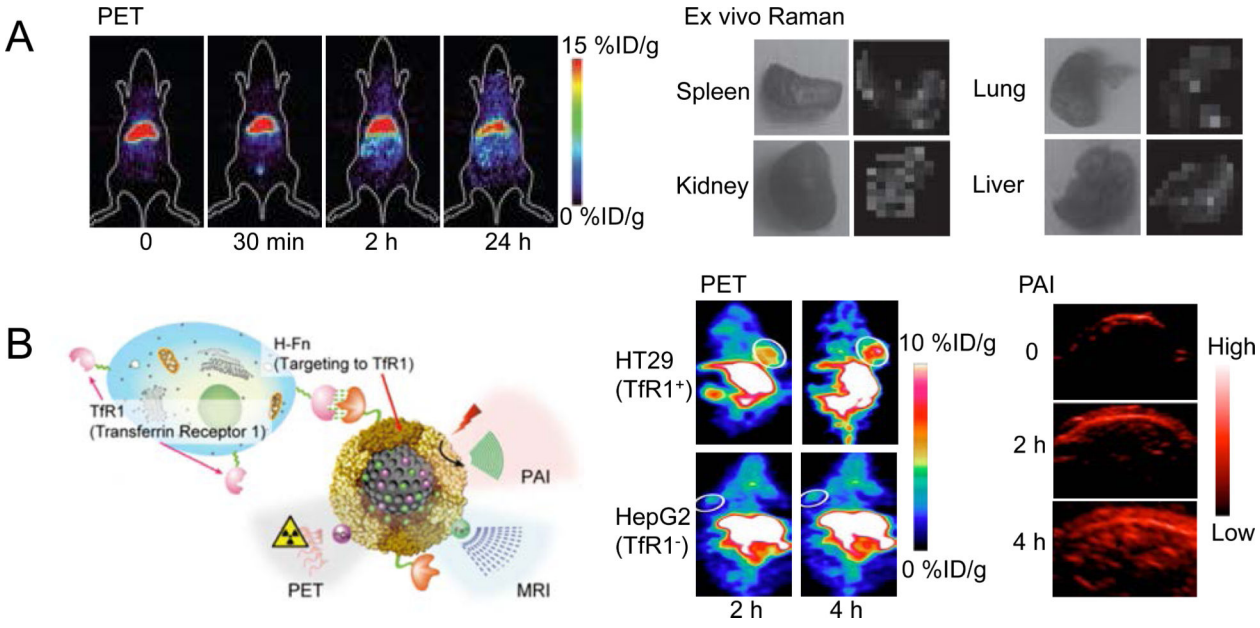

Figure 4.

(A) PET and *ex vivo* Raman imaging to evaluate the organ distribution of ^{64}Cu-labeled gold nanoparticles. Consistent organ uptake was obtained by PET and Raman signals. Adapted with permission (93). (B) ^{64}Cu-labeled melanin nanoparticles were used for tumor detection via PET and PAI. The schematic structure of MNPs is provided along with examples of both PET and PAI images of tumor-bearing mice. Adapted with permission (96).

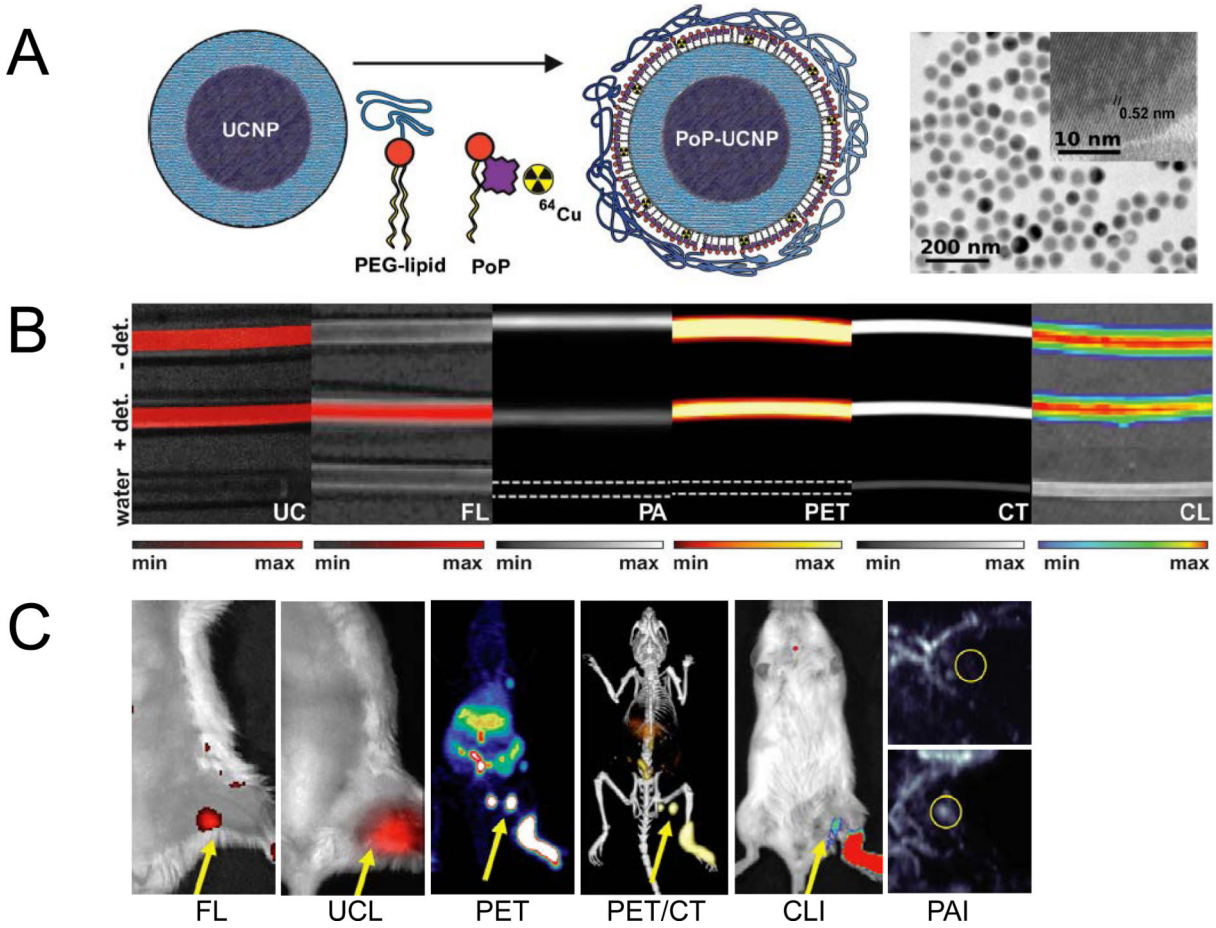

Figure 5.

Hexamodal imaging with radioactive nanomaterials. (A) Schematic structure and TEM images of this porphyrin/lipid wrapped UCNPs. (B) Imaging studies with material-filling tubing by UCL, fluorescence, PAI, PET, CT, and CLI. Signal intensity – tissue depth relationship was also examined. (Note: +/− det means cover or remove turkey breast over the tubing). (C) *In vivo* LN mapping by these six imaging modalities. PA images before and after the material injection are shown. Adapted with permission (103).

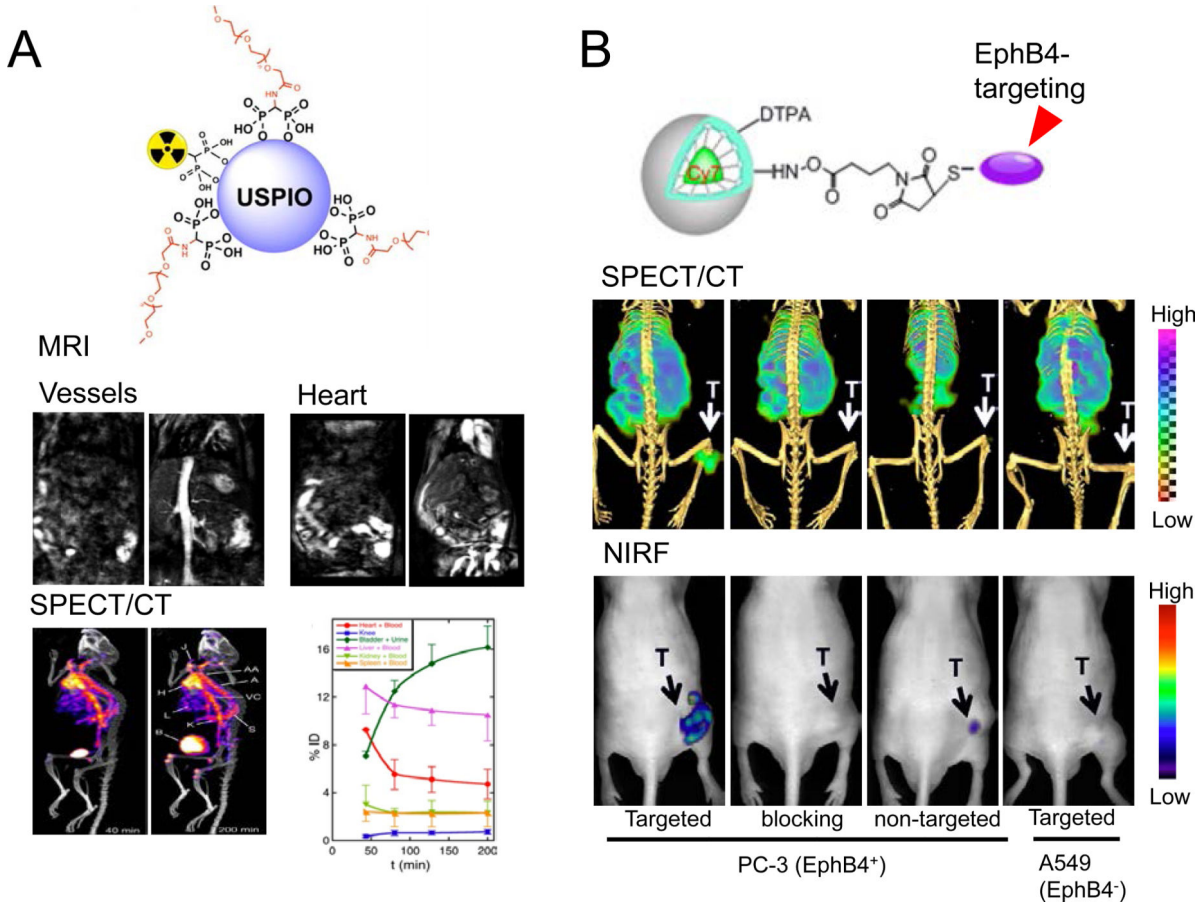

Figure 6.

(A) Schematic structure of ^{99m}Tc-labeled USPIOs (an IONP) and clarification of its organ distribution by SPECT and MRI. T_1-weighted images showing the increase in signal from blood in the vessels and the heart. SPECT/CT demonstrated similar pharmacokinetic profile for the ^{99m}Tc-labeled USPIO. Adapted with permission (111). (B) Schematic structure of EphB4-targeting micelles and their applications in SPECT/NIRF imaging of EphB4^{+} and EphB4^{-} tumors. The EphB4 specificity of these micelles was validated by these two imaging modalities. Adapted with permission (114).

Table 1

Representative radioactive nanomaterials for multimodality imaging.

Core nanomaterials	Physical properties	Radiolabel incorporation method	Intrinsic imaging capacity	Utilization	Synthesis cost	Representative references
Inorganic nanomaterials						
IONPs	Paramagnetic (T_2 contrast, T_1 contrast when size is small)	External chelator, isotope absorption, covalent linkage (^{18}F)	MRI	LN mapping, tumor detection	$	(53, 58-60)
Gold	Fluorescence, photoacoustic signal, SERS	External chelator, radioactive precursor	Fluorescence, PAI, CRET	Tumor targeting, image-guided surgery	$$	(44, 93, 95, 99)
QD	fluorescence	External chelator	Fluorescence, CRET	LN mapping, tumor detection/surgery	$	(79, 80, 89, 90)
Silica	Biocompatibility, ultra-high cargo loading capacity, biodegradability	External chelator, Isotope absorption,	N/A	LN mapping, tumor detection/surgery (for C-Dots), image-guided drug delivery	$	(86, 88)
Carbon nanomaterials	Photothermal, Fluorescence, Photoacoustic signal, Raman signal	External chelator,	Fluorescence	Tumor detection	$$ (fullerene can be $$$)	(25, 112)
UCNPs	luminescent	External chelator, radioactive precursor (doping)	UCL	LN mapping, tumor detection	$$$	(83, 103)
Mn/Gd-containing nanomaterials	Paramagnetic (T_1 contrast)	External chelator, radioactive precursor	MRI	Tumor targeting,	$$	(72, 113)
Organic nanomaterials						
Liposome	Biocompatibility, Optimal pharmacokinetics	External chelator, isotope absorption	Fluorescence, MRI (intrinsic label)	Tumor targeting	$	(68, 115)
Polymers	Biocompatibility, versatile chemistry	External chelator, isotope absorption	Fluorescence, PET (intrinsic label)	Tumor targeting, Image-guided drug delivery	$	(69, 114, 116)